Research Paper

Study on the Effectiveness of Monte Carlo Filtering when Correcting Negative SEA Loss Factors

Paweł NIERADKA[(1), (2)*], Andrzej DOBRUCKI[(1)]

[(1)] *Wrocław University of Science and Technology*
Department of Acoustics, Multimedia and Signal Processing
Wroclaw, Poland

[(2)] *KFB Acoustics, Acoustic Research and Innovation Center*
Domasław, Poland

*Corresponding Author e-mail: p.nieradka@kfb-acoustics.com

The power injection method (PIM) is an experimental method used to identify the statistical energy analysis (SEA) parameters (called loss factors – LFs) of a vibroacoustic system. By definition, LFs are positive real numbers. However, it is not uncommon to obtain negative LFs during experiments, which is considered a measurement error. To date, a recently proposed method, called Monte Carlo filtering (MCF), of correcting negative coupling loss factors (CLFs) has been validated for systems that meet SEA assumptions. In this article, MCF was validated for point connections and in conditions where SEA assumptions are not met (systems with low modal overlap, non-conservative junctions, strong coupling). The effect of removing MCF bias on the results was also examined. During the experiments, it was observed that the bias is inversely proportional to the damping loss factor of the examined subsystems. The obtained results confirm that the PIM, combined with MCF, allows to determine non-negative SEA parameters in all considered cases.

Keywords: statistical energy analysis; coupling loss factor; Monte Carlo filtering; power injection method.

1. Introduction

Statistical energy analysis (SEA) is a numerical method that allows the behavior of vibroacoustic systems to be modeled using a system of linear equations at medium and high frequencies (LYON, DEJONG, 1995). SEA can deal with problems where acoustic and vibrational fields are coupled. SEA is widely used in the automotive industry (noise, vibration, and harshness – NVH) (CHEN *et al.*, 2012) and also when designing silent ships (HATTORI *et al.*, 1985), trains (JI *et al.*, 2015), airplanes (BORELLO, 2018), and buildings (Craik, 1982). Other applications include: predicting the insertion loss of sound-insulating enclosures (NIERADKA, DOBRUCKI, 2018) and machinery noise (LALOR, 1996), estimating the sound reduction index of partitions (PRICE, CROCKER, 1970) and noise in kitchen appliances (ZARATE *et al.*, 2017), damage detection in joints (PANKAJ, 2019), predicting the in-

sertion loss of lagging in ducts (YOGANANDH *et al.*, 2019), and noise transmission in the spacecraft industry (HWANG, 2002).

The vibroacoustic system is fully identified with regard to SEA when parameters called loss factors (LFs) are known. LFs divide into coupling loss factors (CLFs) and damping loss factors (DLFs). Experimental SEA (E-SEA) is a set of methods allowing LFs to be determined using measurements. The most widely used E-SEA method is the power injection method (PIM) (BIES, HAMID, 1980), which is utilized in this paper. Other methods can also be labeled as E-SEA, e.g., identification based on intensity measurements (MING, 1998), mobility measurements (CACCIOLATI, GUYADER, 1994), input power modulation (FAHY, RUIVO, 1997), and the energy ratio method (GU, SHENG, 2015).

Post-processing E-SEA data can occasionally produce negative LFs, which are considered measurement

errors. Two reasons for the occurrence of negative LFs can be distinguished: measurement uncertainty and the failure to meet SEA assumptions. SEA assumptions are widely discussed in the literature (LAFONT *et al.*, 2014) and are shortly summarized in this article. In order to correct negative LFs, the Monte Carlo filtering method (MCF) can be used (DE LAS HERAS *et al.*, 2020). In MCF, a statistical ensemble of energy matrices is generated based on the mean value and variance of the experimental data. Only those members of the ensemble that give correct results are used in the final calculations. HOPKINS (2002) conducted virtual E-SEA experiments, where he used an alternative approach to MCF. Instead of building a statistical ensemble based on measurement variance, he was varying system dimensions and physical properties, which in turn allowed for positive LFs to be obtained for most members of the ensemble. This approach is possible and robust due to the fact that virtual experiments in the FEM framework allowed for the system dimensions and properties to be quickly alternated. LALOR (1990) proposed an alternative formulation of PIM to obtain lower matrix condition numbers. HODGES *et al.* (1987) suggested using matrix fitting methods to correct negative CLFs.

In this work, experiments are performed on steel plates connected using different structural junctions at different levels of damping. Similar structures have been investigated by others, but the research was mainly focused on the values of coupling loss factors. The dependence of CLFs on the type of joint and the type of material was investigated by MANDALE *et al.* (2016), BHAGWAN, POPURI (2019), and others. The dependence of the CLF value on the plate's thickness ratio and the number of points in point junctions has also been experimentally verified (PANUSZKA *et al.*, 2005). Negative CLFs were not considered in those publications. The effectiveness of MCF was experimentally proved for a plate system suspended in a room (acoustics system) and numerically validated for plate ensembles (DE LAS HERAS *et al.*, 2020). This verification only included the effect of measurement uncertainty because it was performed in conditions where SEA assumptions were met.

The authors of the present publication are unaware of any article where MCF was employed for point junctions and in conditions that violate SEA requirements (low modal overlap, non-conservative junctions). Conditions where SEA assumptions are violated are often encountered in industrial and other real-life scenarios, and it is therefore desirable to know how the MCF method will behave in such situations. Assessing the effectiveness of MCF in non-ideal conditions is the main research problem tackled in this publication.

The paper is organized as follows. Section 2 gives a brief introduction to E-SEA, MCF, and SEA assumptions. Section 3 presents the tested systems and describes the course of the measurements. In Sec. 4, the relationships between the results of the MCF procedure and the SEA assumptions are presented for different joints and damping levels. Moreover, the effect of MCF bias on the obtained LFs is investigated. Section 5 summarizes the major findings of the study.

2. Foundations of the applied methods

2.1. Experimental statistical energy analysis

In the SEA approach, the structure (system) is subdivided into a set of subsystems. A subsystem is defined as a group of similar modes of vibration. The structure should be physically divided into parts in places with high impedance mismatches (branches, discontinuities, junctions, changes in material type, and thickness) in order to obtain weak coupling conditions. Both acoustic cavities and elastic solids can be treated as a subsystem.

In SEA, the vibroacoustic system is fully described when the set of LFs parameters are known. LFs are subdivided into DLFs and CLFs. DLFs describe the inner energy dissipation of subsystems, while CLFs describe the energy flow between subsystems.

SEA is based on writing down a set of equations that describe the energy balance between subsystems. Figure 1 shows an example of the energy balance between two subsystems – subsystem 1 with mean energy E_1 and subsystem 2 with mean energy E_2. Furthermore, η_{11} and η_{22} are damping loss factors, η_{12} and η_{21} are coupling loss factors, and $P_{\text{in}1}$ and $P_{\text{in}2}$ are input powers.
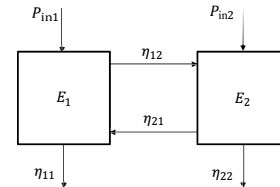

Fig. 1. Energy balance between two SEA subsystems.

The general SEA equation for a system comprising N subsystems can be written down using matrix notation (LYON, DEJONG, 1995):

$$\{P\} = \omega [L]\{E\}, \tag{1$_1$}$$

where $\{P\}$ is a column vector of input powers, $\{E\}$ is a column vector of the (unknown) subsystems' energies, ω is the center angular frequency of the analyzed band $\Delta\omega$ (i.e., octave or 1/3-octave band), and $[L]$ is the loss factor matrix.

The loss factor matrix $[L]$ is constructed as follows:

$$L_{ij} = \begin{cases} \displaystyle\sum_{u=1}^{N} \eta_{iu} & \text{if } i = j, \\ -\eta_{ji} & \text{if } i \neq j, \end{cases} \tag{1$_2$}$$

where $i = 1, ..., N$, $j = 1, ..., N$.

When LFs and input powers are known, determining the unknown energies of subsystems is straightforward, as can be seen in Eq. (1). For complex junctions and structures, LFs are often unknown and need to be identified.

Experimental SEA is a set of methods allowing to determine the LFs of a vibroacoustic system. In this work, we focus on a method derived directly from the energy balance equations. Equation (1) can be rewritten and modified so that the LFs (matrix $[L]$) become unknowns:

$$[L] = [P] [E]^{-1} / \omega, \qquad (2)$$

where $[P]$ is the input power matrix and $[E]$ is the energy matrix. This is called the power injection method (BIES, HAMID, 1980). During the experiments, input powers and the subsystems' energies have to be obtained. Each subsystem is excited separately (the power is injected), and the responses are measured simultaneously on every subsystem in order to match the number of equations with the number of unknowns. The consequence is that vectors $\{E\}$ and $\{P\}$ in Eq. (1) become matrices $[E]$ and $[P]$ in Eq. (2). $[E]$ matrix entries E_{ij} stands for the energy of subsystem i when subsystem j is excited. $[P]$ is a diagonal matrix with entries P_{jj}, which stands for the power injected into subsystem j.

In order to obtain LFs, the energy matrix needs to be inverted. Since the input force has a form of the Dirac impulse in the time domain, actual powers and energies as in Eqs. (1) and (2) cannot be utilized. Instead, equivalent input powers and energies (normalized to force autospectrum) in frequency band $\Delta\omega = \omega_2 - \omega_1$ can be determined based on transfer function measurements as follows:

$$P_{\Delta\omega, eq} = \frac{1}{\omega_0} \text{Im} \left[\int_{\omega_1}^{\omega_2} H_{af}(\omega) \, d\omega \right], \qquad (3)$$

$$E_{\Delta\omega, eq} = M \frac{1}{\omega_0^2} \int_{\omega_1}^{\omega_2} |H_{af}(\omega)|^2 \, d\omega, \qquad (4)$$

where ω_0 is the center frequency of $\Delta\omega$, H_{af} is the transfer function between acceleration and the input force, and M is the mass of the subsystem. From Eqs. (3) and (4), it is only possible to determine the effective powers and energies that are normalized to the force autospectrum and not the actual powers and energies. Note that the imaginary part and the division by ω are used to compute the input power. The reason is that during measurement, acceleration is obtained, but in calculations, velocity is used. A transfer function H_{af} in Eq. (3) is taken between the force and acceleration in the driving (excitation) point. In Eq. (4), acceleration is taken from random points in the structure away from the driving point and subsystem boundaries (in order to avoid contributions of direct and evanescent waves).

It is possible to further normalize energy matrix $[E]$ in Eq. (2) in terms of input power in order to obtain normalized energy matrix $[G] = \omega[E][P]^{-1}$. It was shown that this could lead to a better matrix condition number (DE LAS HERAS *et al.*, 2018). The formula can now be written as:

$$[I] = [L] [G], \qquad (5)$$

where $[I]$ is an identity matrix. The variant of PIM that uses the $[G]$ matrix is known in the literature as normalized energy matrix inversion (NEMI). The loss factor matrix $[L]$ in NEMI is computed by inverting $[G]$:

$$[L] = [G]^{-1}. \qquad (6)$$

After the inversion, LFs can be directly extracted from $[L]$ as follows: 1) coupling loss factor η_{ij} is off-diagonal term L_{ji} multiplied by -1, and 2) damping loss factor η_{ii} is obtained by summing the elements of column i.

The procedure described above needs to be repeated for each frequency band of interest.

2.2. Monte Carlo filtering

The inverse energy matrix obtained from measurements will not always provide only positive LFs. SEA matrices are very sensitive to measurement uncertainties (DE LAS HERAS, 2018). One of the ways to solve this is to use MCF, which was proposed by DE LAS HERAS (2020). A similar approach, proposed by BOUHAJ (2017), was utilized to assess CLFs uncertainties. The general idea of MCF is presented in Fig. 2.
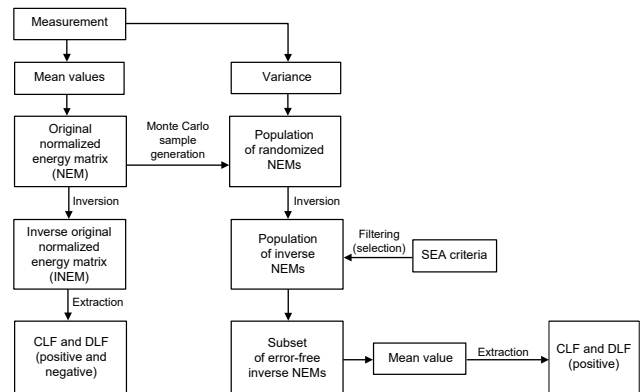

Fig. 2. Monte Carlo filtering procedure.

The classical E-SEA approach (as described in Subsec. 2.1) is presented in the first column of the graph in Fig. 2. In the MCF approach, the population of randomized NEMs is generated by using the original NEM and the measurement variance. The population is then filtered in order to remove all matrices that will produce negative LFs. The final step is to compute the mean value of the obtained LFs. More details

on using this method can be found in reference articles (DE LAS HERAS *et al.*, 2020; BOUHAJ *et al.*, 2017).

This article provides an extended MCF validation for a wide range of technical junctions. The validation includes the following steps: 1) the influence of violating SEA assumptions on MCF results, 2) the influence of the sample bias on MCF results.

2.3. SEA assumptions

The SEA assumptions are as follows (LE BOT, 2015): 1) a high modal overlap factor; 2) weak coupling between subsystems; 3) non-conservative junctions; 4) a high number of modes in frequency bands; 5) a diffuse field; 6) uncorrelated white noise excitations; 7) statistically independent modes; 8) negligible non-resonant transmission.

In this publication, we mainly focus on the first three assumptions. This approach is justified due to the fact that assumption 1 is often referred to as the most crucial requirement (CULLA, SESTIERI, 2006).

Assumption 1 states that:

$$\mu \gg 1, \tag{7}$$

where μ is the modal overlap factor, which is defined as:

$$\mu = n\omega\eta, \tag{8}$$

where n is the modal density, ω is the angular frequency, and η is the DLF. Modal density can be estimated by equation (LE BOT, 2015):

$$n = \frac{2M\langle \mathrm{Re}\{Y\}\rangle_{A,\omega}}{\pi}, \tag{9}$$

where M is the mass of the subsystem, Y is the driving point mobility, and $\langle...\rangle_{A,\omega}$ stands for space and frequency averaging. Equation (9) is useful because variables from the right side of the equation can be obtained from modal hammer measurements performed during PIM. A high modal overlap results in a smooth frequency response function, which is not dominated by any resonance. This is crucial because SEA was derived with the assumption of the equipartition of modal energy, where each resonant mode is of equal importance when computing energy flow.

Smith's criterion (SMITH, 1979) can be used to check assumption 2 and states that:

$$\gamma \ll 1, \tag{10}$$

where γ is called the coupling strength indicator, which can be computed by taking the ratio of CLFs to DLFs. In this study, Smith's criterion is used, but it must be noted that other criteria for coupling strength can be found in the literature (FINNVEDEN, 2011).

Non-conservative junctions are an idealization that never exists in practice. One can say that assumption 3 is always violated to some extent because even welding junctions introduce some damping to the system. In practice, this effect is neglected, apart from when the losses associated with the joint are comparable to the losses of the entire system. For example, a joint that does not meet assumption 3 may be the 6 mm thick rubber pads that were used in the experiments.

Assumption 4 can be written as:

$$N_{\Delta\omega} \gg 1, \tag{11}$$

where $N_{\Delta\omega}$ is the number of modes in frequency band $\Delta\omega$, and $N_{\Delta\omega}$ can be counted directly when modes are distinguishable. This is usually not the case for high frequencies, and one can use the approximate formula:

$$N_{\Delta\omega} = n\Delta\omega. \tag{12}$$

Assumption 4 in the present research is fulfilled for all systems.

Assumption 5, in some sense, stands in opposition to assumptions 1 and 2. In assumptions 1 and 2, a high damping loss factor is desirable, but in assumption 5, a low damping loss factor is desirable in order to ensure diffuse field conditions. The following requirement for the normalized attenuation factor $\overline{m}$ can be checked to test diffuse field conditions:

$$\overline{m} \ll 1. \tag{13}$$

The normalized attenuation factor is computed by using the equation:

$$\overline{m} = \frac{\eta\omega}{c_g}\overline{l}, \tag{14}$$

where c_g is the group speed, and $\overline{l}$ is the mean-free-path, which for 2D subsystems is equal to

$$\overline{l} = \pi\frac{A}{S}, \tag{15}$$

where A and S are the surface area and perimeter of the subsystem, respectively.

Inequality (Eq. (13)) assures that rays will experience few reflections before being attenuated by the internal damping mechanisms of the subsystem. Assumption 5 is violated for all the considered high-damped systems above 2500 Hz.

Assumption 6 is always fulfilled in this research by using modal hammer impulses that provide a wideband uniform spectrum in the frequency range of interest.

Assumption 7 can be fulfilled by using rain-on-the-roof excitation. In the present research, this excitation is reproduced by performing spatial averaging for point excitations, which is standard practice (CIMERMAN *et al.*, 1997).

Assumption 8, in practice, could be violated in some circumstances (e.g., highly damped systems, mass law transmission), but this effect is not further analyzed here.

3. Experiments

The investigated systems were steel plates connected to each other at a right angle. The mechanical and geometrical parameters of the plates are shown in Table 1. The studied objects contained holes that were made for free suspension. The diameter of the holes was 23 times smaller than the smallest considered flexural wavelength in the system (7 cm), so it can therefore be assumed that the influence of the holes is negligible in the frequency range of interest.

Table 1. Geometric and mechanical parameters of the tested structure.

Geometry		Photo
Thickness	2 mm	
Length	0.49 m	
Width	0.49 m	
Mechanical parameters		
Material	Steel DC03	
Density	7827 kg/m^3	
Young's modulus	205 GPa	
Poisson number	0.3	

The plates were measured for three damping levels (low, medium, and high) in order to vary the modal overlap factor. Rubber magnetic tape was used to introduce damping to the plates (Fig. 3).
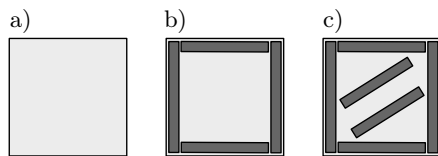

Fig. 3. Tested plate with: a) low damping; b) medium damping; c) high damping.

The plates were connected by different structural junctions (Fig. 4). The line junctions included a line weld junction and a rubber connection. The point junctions used in this research were: point welding, bolts, and rivets. The point junctions consisted of three points evenly distributed along the common edge of the plates.
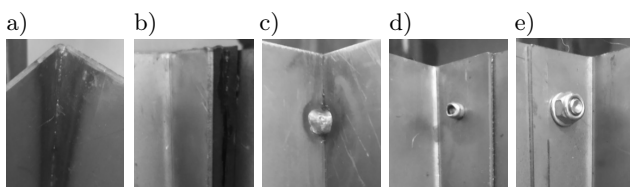

Fig. 4. Technical junctions used to connect the plates: a) line welding; b) rubber connection; c) point welding; d) rivets; e) bolts.

The panels were hung freely on elastic lines. The modal hammer PCB 086C03 was used to excite the struc-tures, the PCB 356A03 accelerometer was used to measure the source subsystem response in the driving point, and PCB T356A32 accelerometers were used to measure the source and receiver subsystem response away from the excitation points. HEAD acoustics SQuadriga II was used for data acquisition. The sensors were bonded to the structure using wax.

For averaging purposes, three excitation and six response points were randomly chosen on each subsystem. Only the "z" component of acceleration was registered during the experiments (this research focuses on a bending wave transmission, so only out-of-plane wave motion was crucial).

The post-processing script was written in the Python programming language. Based on the obtained signals from the sensors, the input powers and energies were determined using Eqs. (3) and (4). Then, the procedure described in Subsec. 2.1 was followed to obtain the LFs. Some loss factors were negative, which justified the use of the MCF described in Subsec. 2.2.

4. Results and discussion

4.1. Correction of negative CLFs

In this section, a detailed analysis is conducted on the impact of meeting SEA conditions on the effectiveness of the MCF method. A logarithmic scale was used to present the data in graphs, and it was therefore not possible to represent the actual values of negative numbers. Instead, negative CLFs are represented symbolically with gray markers as the mean value of adjacent positive CLFs. The graphs associated with the SEA assumptions also appear in this section. The gray areas appearing on these graphs indicate the frequency ranges where the SEA assumptions are not met. Gray areas indicate regions where $\gamma < 1$ and $\mu > 1$ (we set $\gamma = 1$ and $\mu = 1$ as threshold values). Nevertheless, one must keep in mind that the requirements are $\gamma \ll 1$ and $\mu \gg 1$, and other choices of threshold values are possible (e.g., $\gamma = 0.1$ and $\mu = 10$). In order to avoid complications in the analysis, only the direction from subsystem 1 to subsystem 2 is considered. Loss factors η_{21} and η_{22} are not shown in the plots. This is a simplification because some examined junctions are not fully symmetrical. Complete results, including the LFs for the opposite direction, are included in the summary table in Subsec. 4.1.4.

4.1.1. Line welding

In this section, the results obtained for the line welding junction are analyzed. Figures 5, 6, and 7 show the relation between the sign of the obtained loss factors and SEA assumptions for low, medium, and high damping, respectively. Figure 8 shows the identification results for all the damping levels.
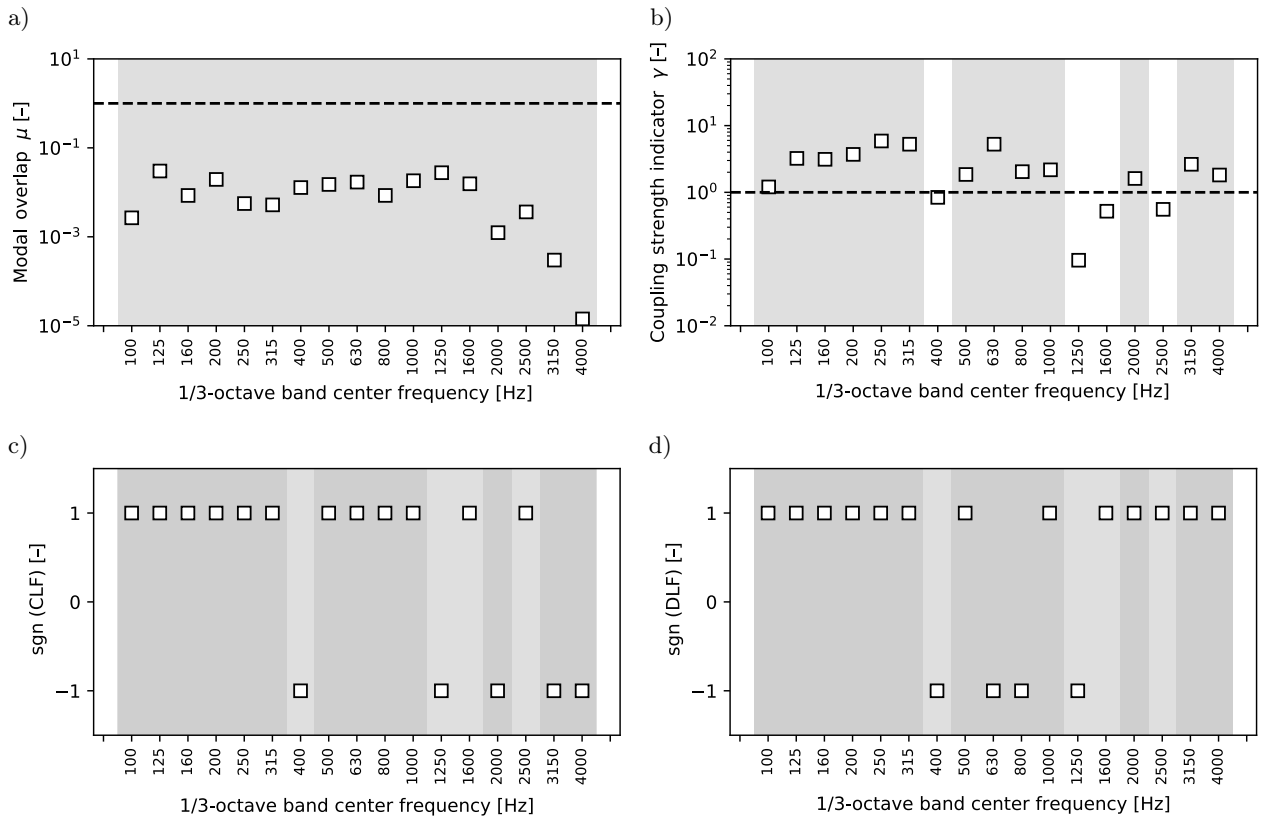
Fig. 5. Influence of the modal overlap (a) and coupling strength (b) on signs of the CLFs (c) and DLFs (d) for the line welding at low damping.
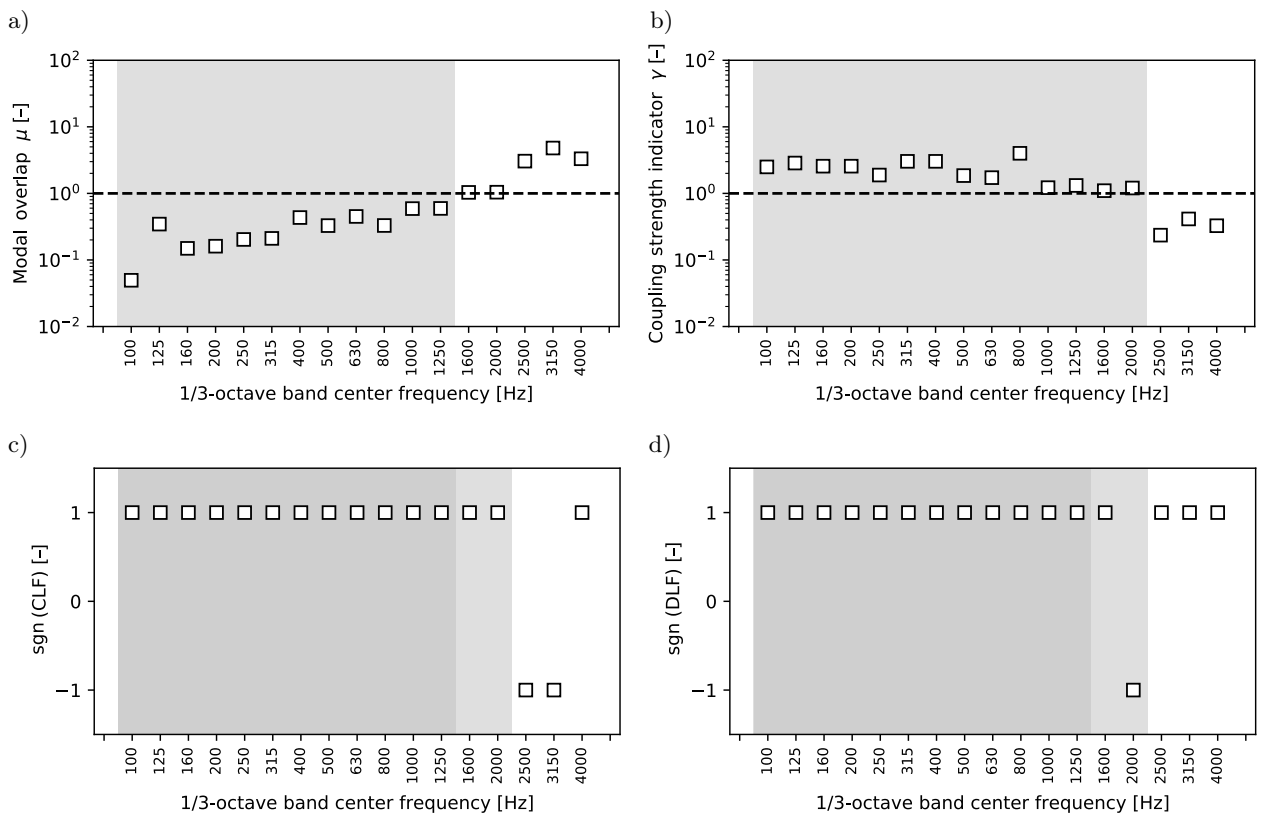

Fig. 6. Influence of the modal overlap (a) and coupling strength (b) on signs of the CLFs (c) and DLFs (d) for the line welding at medium damping.
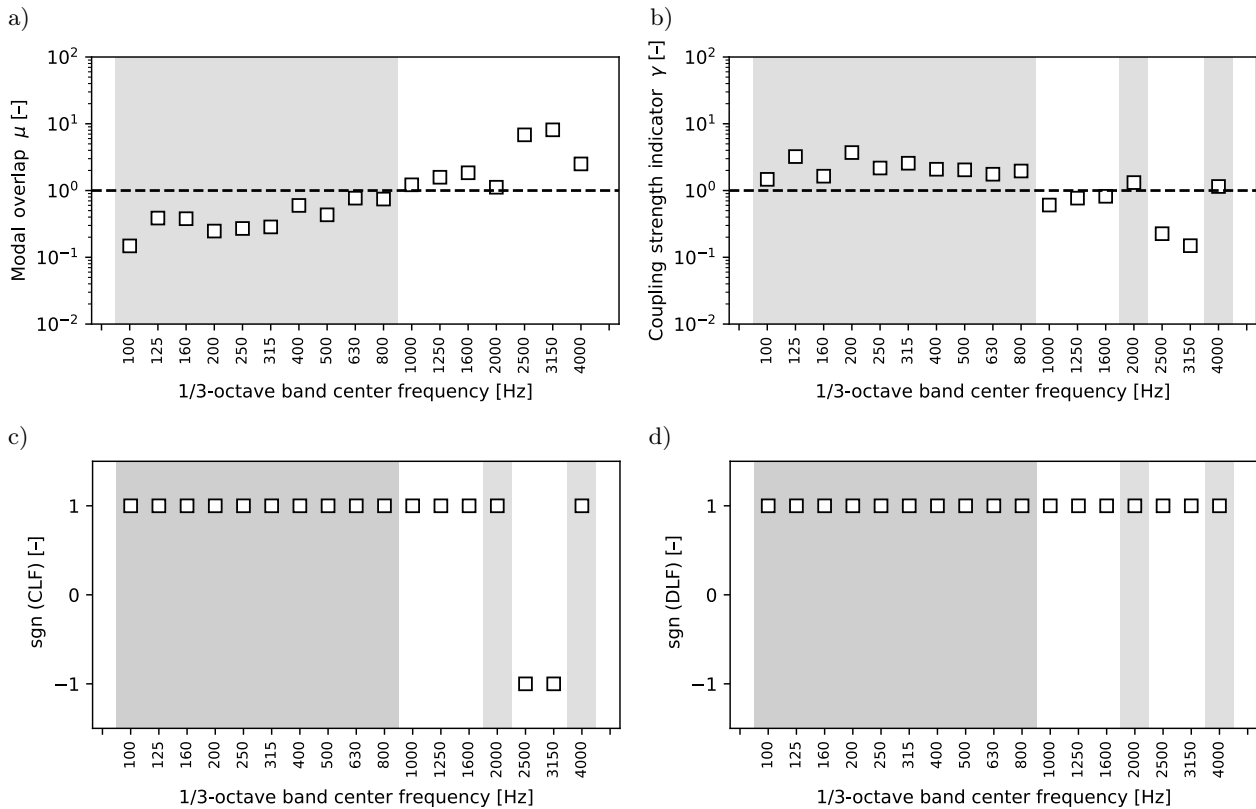
Fig. 7. Influence of the modal overlap (a) and coupling strength (b) on signs of the CLFs (c) and DLFs (d) for the line welding at high damping.

One can notice that as the damping increases, the requirement for the modal overlap is fulfilled in a wider frequency range (Figs. 5a, 6a, 7a). Nevertheless, the requirement for coupling strength is only met in a few bands (Figs. 5b, 6b, 7b). The line weld connects the plates continuously along the common line, which results in high transmission, in turn creating strong coupling conditions (even for the high damped system – Fig. 7b). This allowed (for medium and high damping) the frequency region to be isolated where only one SEA assumption is violated, namely coupling strength.

Negative LFs were obtained for the systems with low, medium, and high damping (Figs. 8a, 8c). All negative LFs were successfully corrected (Figs. 8b, 8d). The biggest amount of negative LFs occurred for the low damped system in the frequency region with a low modal overlap and high coupling strength indicator (Figs. 5c, 5d). This case is difficult to analyze because many unfavorable factors act simultaneously. For the medium and highly damped structures, a few negative LFs were determined within the frequency range for which the SEA assumptions are met (Figs. 6c, 7c). A single DLF was also designated within the frequency region in which the coupling is strong and the modal overlap is high (Fig. 6d). In this case, obtaining negative LFs could result from the measurement uncertainty or strong coupling.

By comparing Fig. 8a with 8b, and 8c with 8d, it can be seen that the MCF procedure used for the low damped system significantly altered the CLF and DLF curves. In turn, for the medium and highly damped system, the MCF provided a smoothing effect while at the same time keeping the values similar.

It is interesting to note that the CLF for the low damping is lower than the CLFs obtained for the medium and high damping. This can be counterintuitive because, in classical SEA, CLFs are independent of DLFs. A lack of dependence on DLFs is assumed in theoretical SEA when CLFs are derived based on wave theory. However, it was shown that CLFs derived using a more precise modal approach do indeed depend on DLFs. This can be observed in the frequency region, where the DLF approaches zero (Yap, Woodhouse, 1996).

4.1.2. Rubber connection

In this section, the results obtained for the rubber junction are analyzed. Figures 9, 10, and 11 show the relation between the sign of the obtained loss factor and SEA assumptions for the low, medium, and high damping, respectively. Figure 12 shows the identification results for all the damping levels.

Rubber constitutes a non-conservative junction, so the connection itself violates SEA assumptions. On the
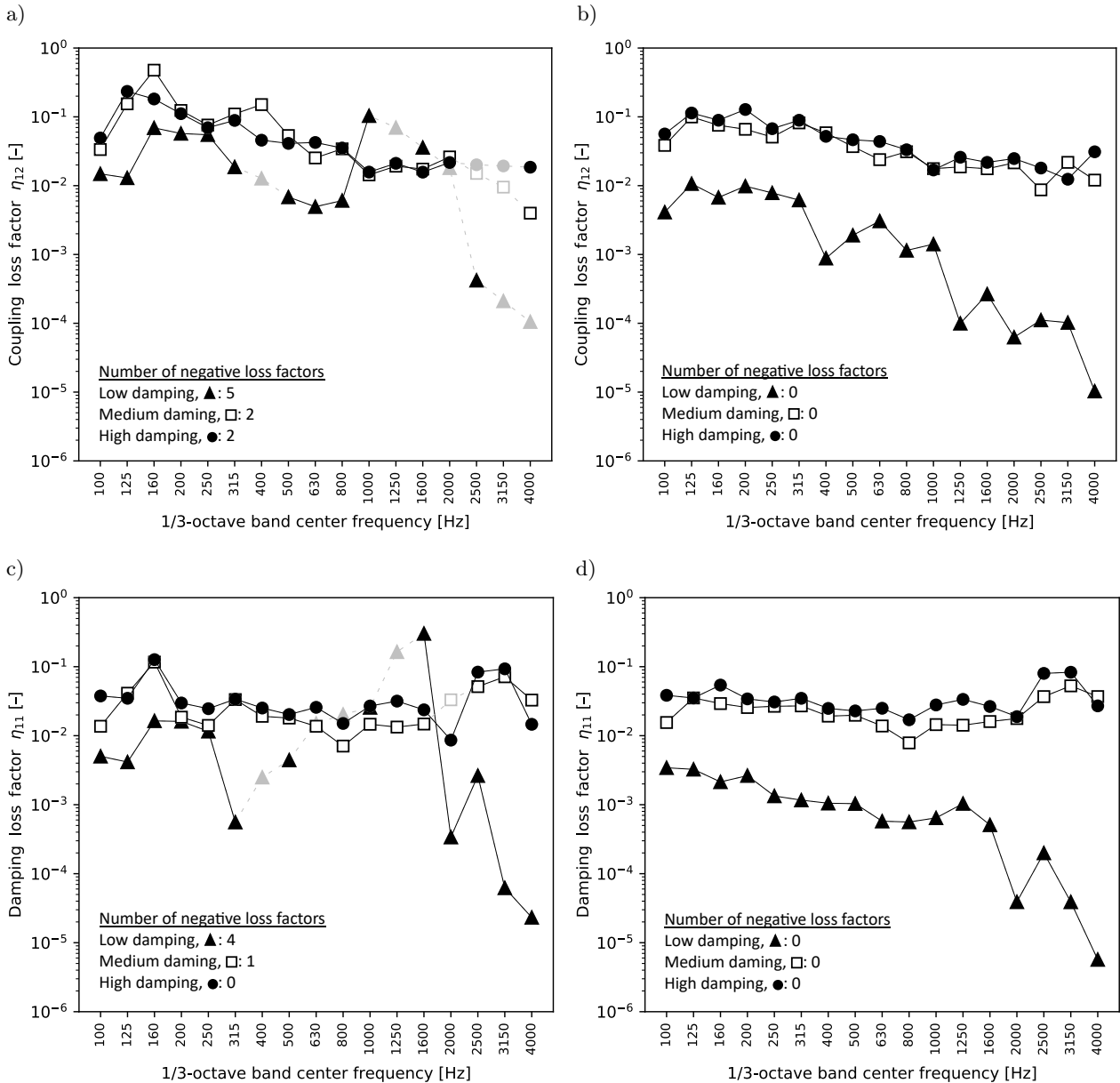
a)

b)

c)

d)

Fig. 8. Identification results for the line welding at all damping levels: a) CLFs without MCF; b) CLF with MCF; c) DLFs without MCF; d) DLF with MCF.

other hand, requirements for the modal overlap and coupling strength were much easier to meet for the rubber junction when compared to the line welding. A non-conservative junction (dissipation of energy in the rubber) resulted in an apparent DLF increase, which helped to obtain a high modal overlap μ. For low damping, μ was higher when compared to the line welding case but still below unity for all the frequency bands (Fig. 9a). For high damping, μ was larger than unity above 315 Hz (in the case of line welding, μ was larger than unity above 800 Hz), as shown in Fig. 11a. The weak coupling condition was easy to obtain thanks to the large compliance of the rubber (Figs. 9b, 10b, 11b), which allowed the frequency range in which only one requirement was not met to be iso-

lated, namely the conservative junction requirement. Nevertheless, no negative LF was determined in this frequency range.

Negative LFs were only identified for the low damped system (Figs. 12a, 12c), and were successfully corrected (Figs. 12b, 12d). Negative values lie in the region where the condition for coupling dissipation is not met (for visual purposes, in Figs. 9c and 9d, this region is not grayed out) and the modal overlap is below unity. Thus, the obtained negative LFs are probably the effect of the non-conservative junction, measurement uncertainty, or low μ.

By comparing Fig. 12c with 12d, it can be seen that the MCF introduced a slight smoothing effect on the obtained DLFs.
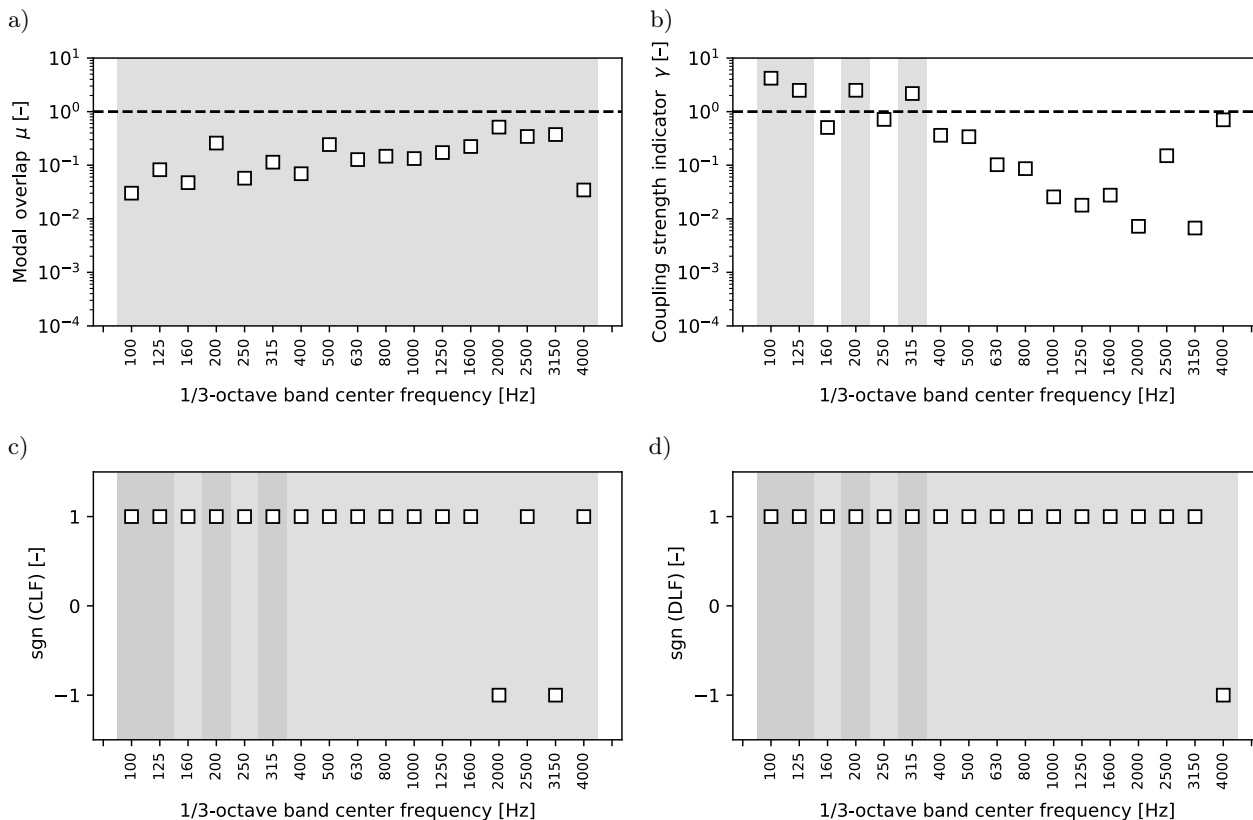
Fig. 9. Influence of the modal overlap (a) and coupling strength (b) on signs of the CLFs (c) and DLFs (d) for the rubber connection at low damping.
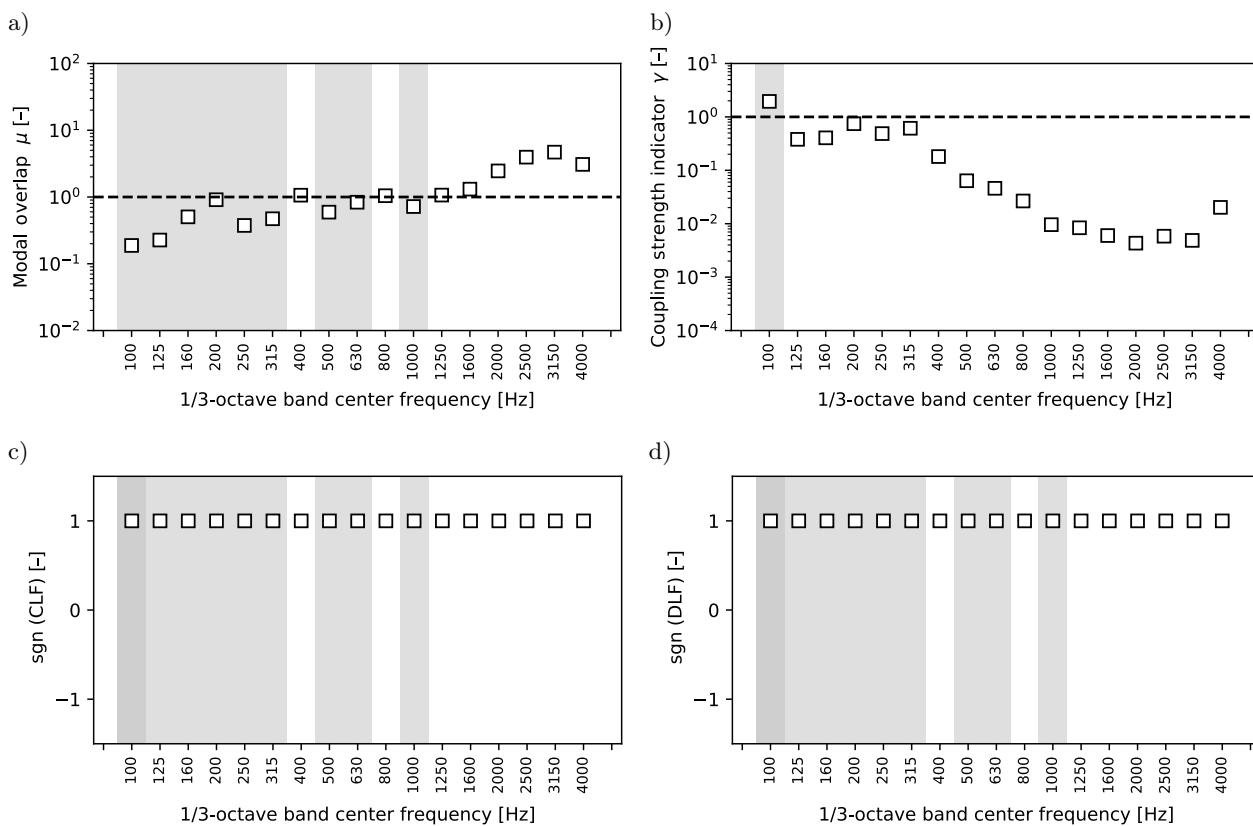

Fig. 10. Influence of the modal overlap (a) and coupling strength (b) on signs of the CLFs (c) and DLFs (d) for the rubber connection at medium damping.
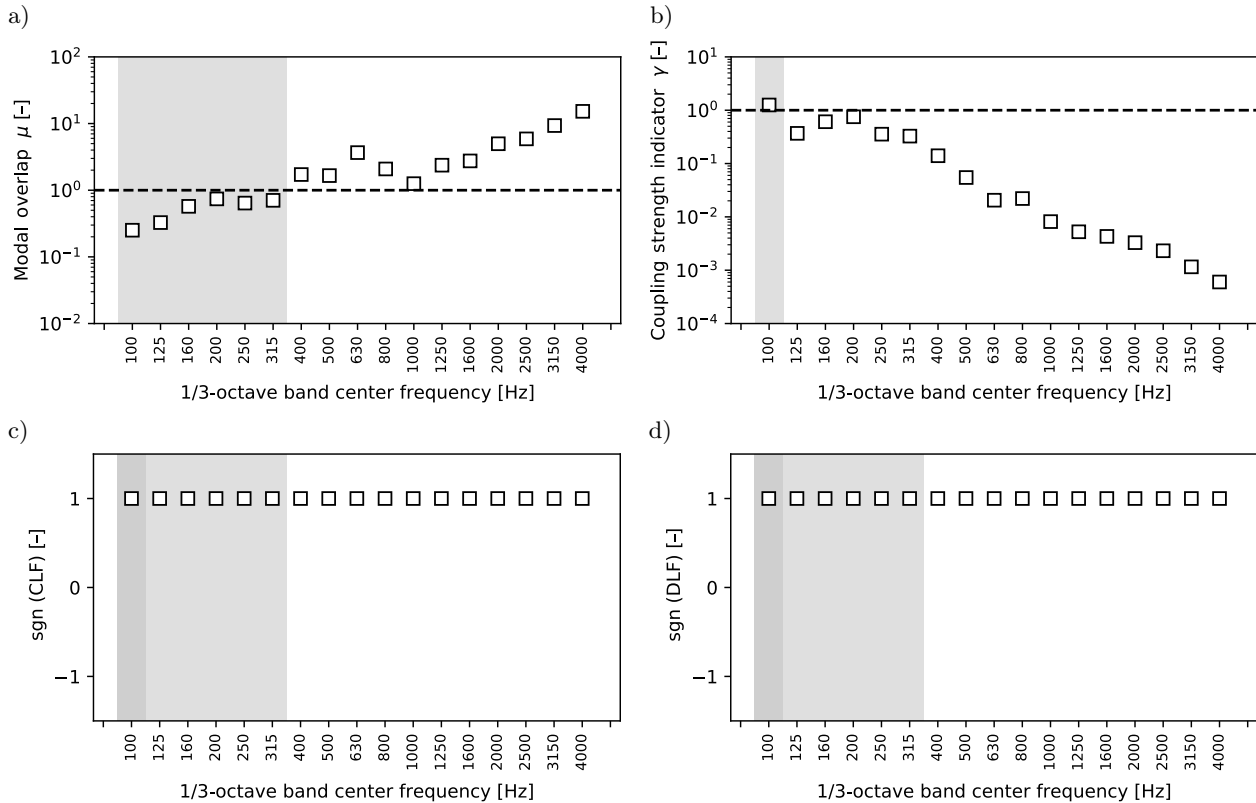
Fig. 11. Influence of the modal overlap (a) and coupling strength (b) on signs of the CLFs (c) and DLFs (d)
for the rubber connection at high damping.

The CLFs obtained for the rubber junctions were the smallest ones in this research. Nevertheless, the usefulness of this kind of junction can be seen to be limited due to the fact that much stiffer joints are required in many technical applications.

4.1.3. Point connections

In this section, the results obtained for the point junctions are analyzed. Figures 13, 14, and 15 show the relation between the sign of the obtained loss factor and SEA assumptions for the point welding, rivets, and bolts, respectively. Figure 16 shows the identification results for all the examined point connections at high damping.

The point connections were approximately non-conservative and provided a weak coupling in a wide frequency range (Figs. 13b, 14b, 15b). Weak coupling was easier to obtain when compared to the line junction cases because the systems were only connected at 3 points. Additionally, all the systems with point connections were highly damped, which resulted in a high modal overlap (Figs. 13a, 14a, 15a). Such conditions seem to be ideal in the case of SEA.

However, even under favorable conditions, a single negative CLF was observed for the system with point welding at 2500 Hz (Fig. 16a, gray arrows). This point lies in the region where all the SEA assumptions are met (Fig. 13c), except for assumption 5.

Thus, the error is probably connected with measurement uncertainty or a lack of diffuse field conditions. As shown in Fig. 16b, the negative value was successfully corrected.

By comparing Fig. 16a with 16b, and 16c with 16d, one can state that the MCF did not introduce much distortion in the final results.

The CLF values for all the point connections are similar, but some differences can be noticed. Figure 16b shows that bolted junctions provide the highest vibration transmission in the low-frequency range. Conversely, the biggest vibration reduction in a wide frequency range can be obtained with rivets.

4.1.4. Results in the opposite directions

Subsections 4.1.1, 4.1.2, and 4.1.3 focused on the LFs obtained for the direction from subsystem 1 to subsystem 2. In general, the tendencies described in the previous subsections also apply to the 2–1 direction, even though some systems were not ideally symmetrical. The CLFs obtained for both directions were similar (Fig. 17). The total number of corrected LFs (including both directions) is summarized in Table 2.

4.2. Influence of the MCF bias

In Fig. 18, the result of the MCF simulation is shown. Each dot in the figure represents a randomized
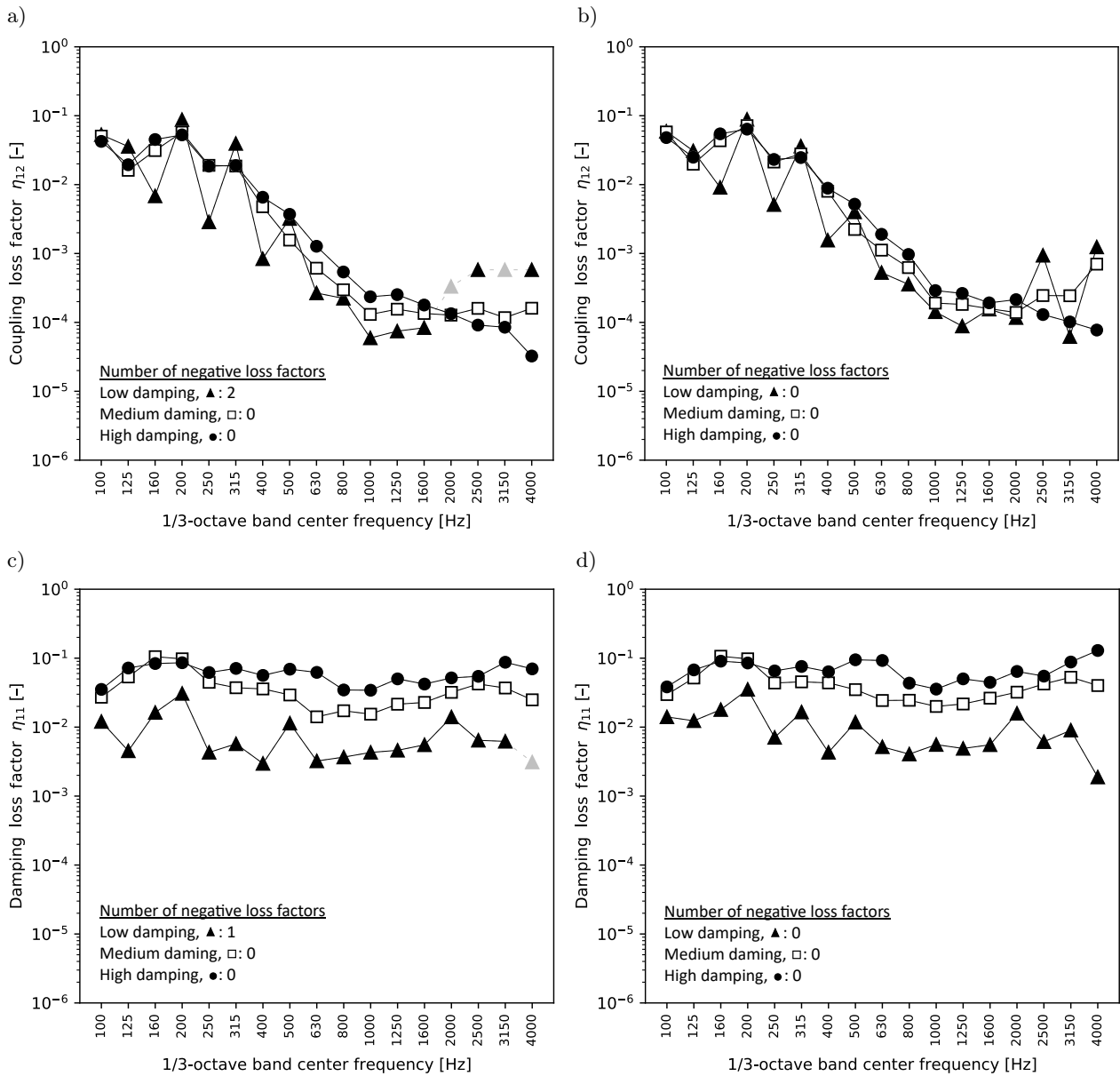
a)

b)

c)

d)

Fig. 12. Identification results for the rubber connection at all the damping levels: a) CLFs without MCF; b) CLF with MCF; c) DLFs without MCF; d) DLF with MCF.

Table 2. Effectiveness of the MCF in correcting negative LFs (both directions included).

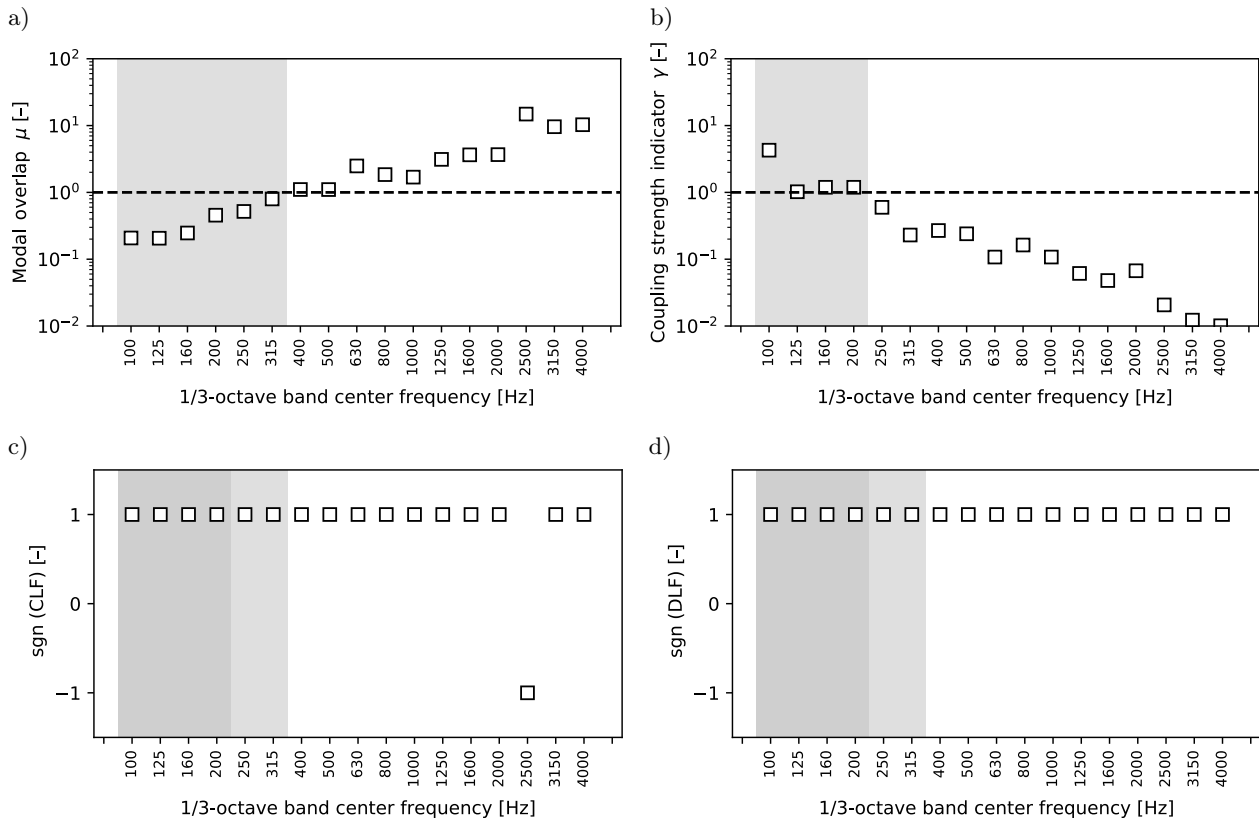| Junction type	Damping	Corrected negative CLFs	Corrected negative DLFs
Line weld	Low	7 → 0	15 → 0
Line weld	Medium	2 → 0	4 → 0
Line weld	High	2 → 0	1 → 0
Rubber	Low	2 → 0	2 → 0
Rubber	Medium	0 → 0	0 → 0
Rubber	High	0 → 0	0 → 0
Point welding	High	1 → 0	0 → 0
Bolts	High	0 → 0	0 → 0
Rivets	High	0 → 0	0 → 0

a)

b)

c)

d)

Fig. 13. Influence of the modal overlap (a) and coupling strength (b) on signs of the CLFs (c) and DLFs (d)
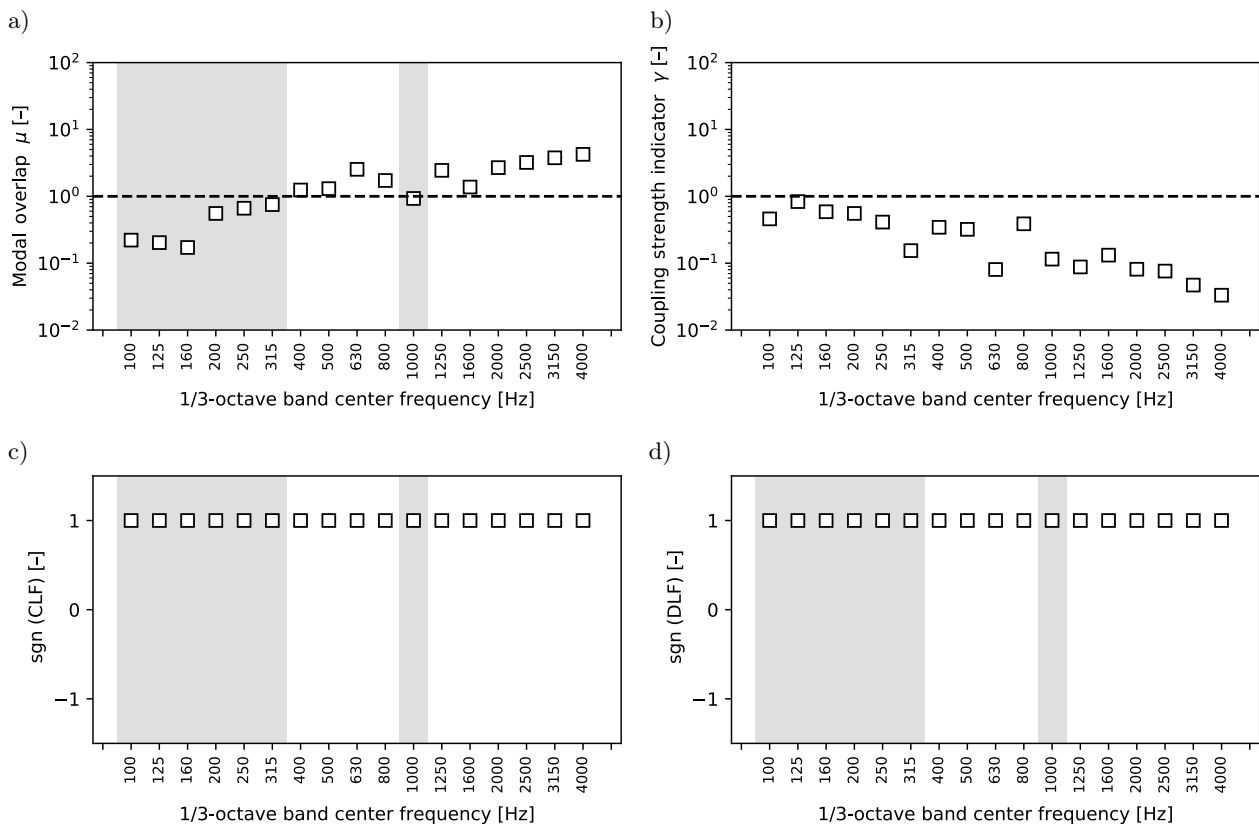for the point welding at high damping.

a)

b)

c)

d)

Fig. 14. Influence of the modal overlap (a) and coupling strength (b) on signs of the CLFs (c) and DLFs (d)
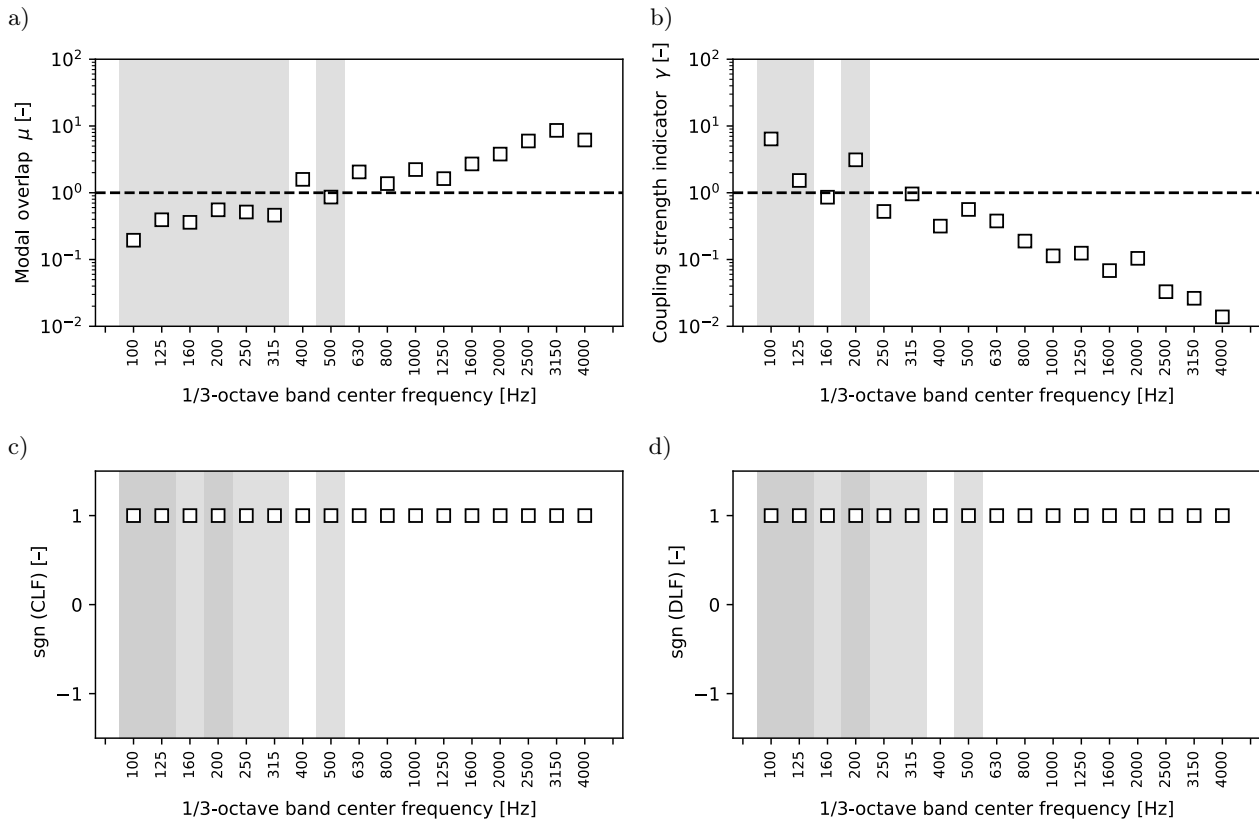for the rivets at high damping.

Fig. 15. Influence of the modal overlap (a) and coupling strength (b) on signs of the CLFs (c) and DLFs (d) for the bolts at high damping.

SEA matrix generated in the Monte Carlo simulation. The black dots represent correct SEA matrices, and the gray dots show incorrect matrices (giving negative LFs). The dots that are closer to zero represent the matrices closer (more similar) to the original matrix. Many norms can be used to compute the distance between the original matrix and individual sample matrices. In this work, the Frobenius norm is utilized. The matrix population generated according to instructions from (BOUHAJ et al., 2017) was based on measurement variance and characterized by the normal distribution to simulate a typical measurement process.

When MCF is performed on experimental data, the so-called bias appears. When the bias is present (Fig. 18a), several incorrect matrices can be found in the original matrix's vicinity (distance close to zero). Such bias is a result of the fact that the measurement is not providing the real expected value but only the approximate mean value. It is possible to remove the bias (Fig. 18b) by performing the second iteration of the MCF.

After removing the bias for the highly damped system with the line weld junction, the CLF decreased slightly in most frequency bands (Fig. 19b). The DLF was less sensitive to this operation (Fig. 19d). The CLF computed with and without removing the bias was compared with the FEM simulation results of this system. Slightly better convergence with the FEM sim-

ulation for most frequency bands was observed for the CLF computed without the bias (Fig. 20). The possible explanation for this can be that after removing the bias, a better average value can be obtained due to the fact that more correct samples are generated. This can be easily observed for the frequencies and systems with larger biases. Figure 21a shows the bias for the 2500 Hz frequency band of the low damped system with line welding. There is only a single "thin line" of correct matrices. Removing bias (Fig. 21b) resulted in significantly more correct matrices that were concentrated around the distance equal to 0. The change in the CLF for a low damped system is also more apparent (Fig. 19a). The same tendencies were observed for the rubber and point junctions, and it therefore seems reasonable to recommend removing the bias when performing MCF.

5. Conclusions

An extended validation of the MCF method was conducted, which can be considered the main contribution of this article. The validation included the following steps: 1) the influence of violating SEA assumptions on MCF results, and 2) the influence of the sample's bias on MCF results. Negative LFs occurred for frequency ranges where SEA assumptions were both
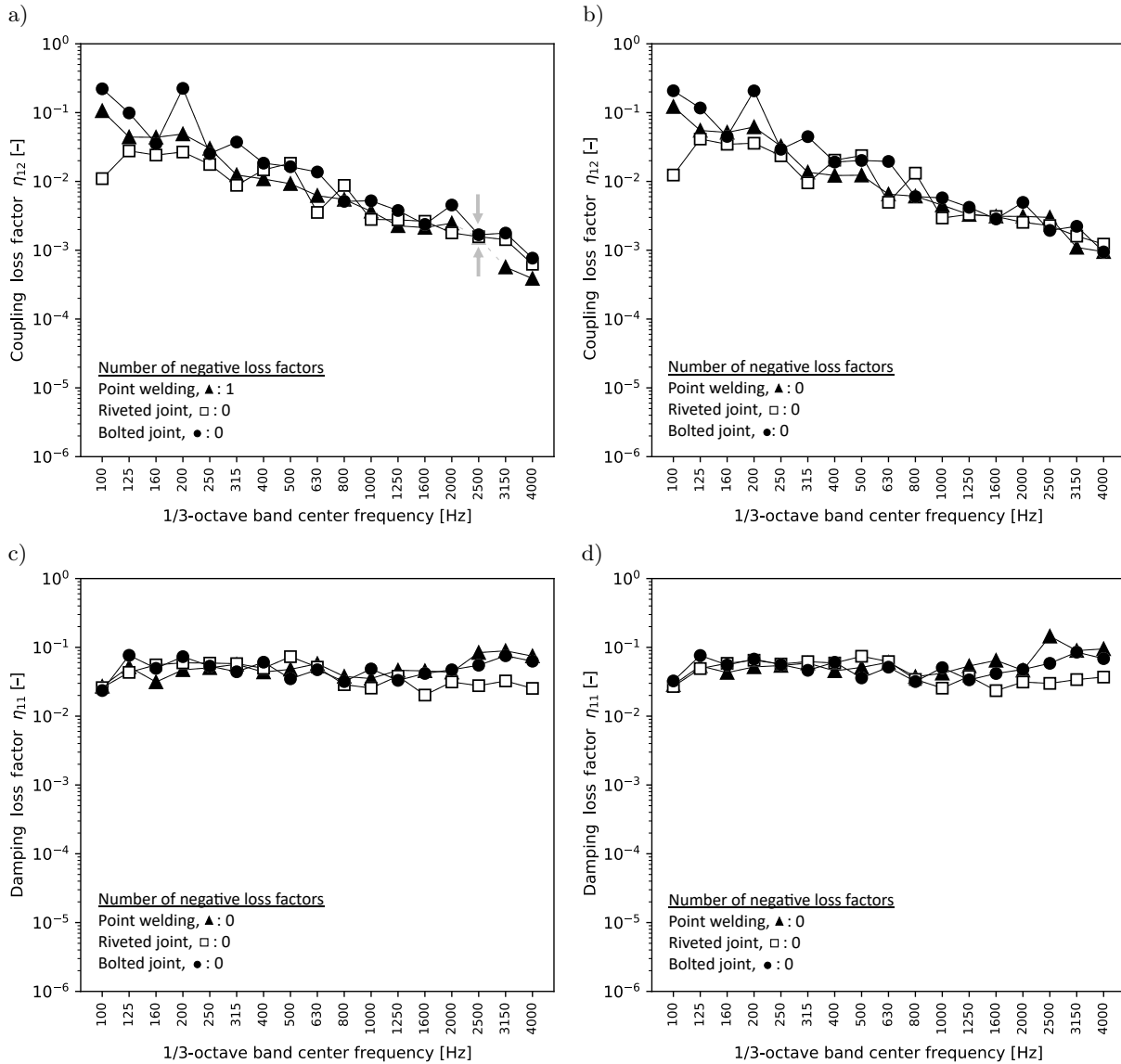
a)

b)

c)

d)

Fig. 16. Identification results for the point junctions: a) CLFs without MCF; b) CLF with MCF;
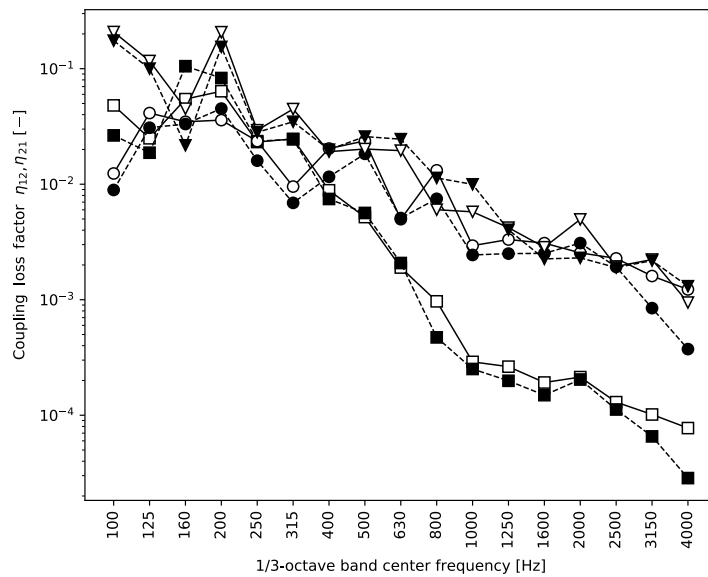c) DLFs without MCF; d) DLF with MCF.

Fig. 17. CLFs in two directions for non-symmetrical systems: rubber (■ and □), rivets (• and ○), bolts (▼ and ▽).
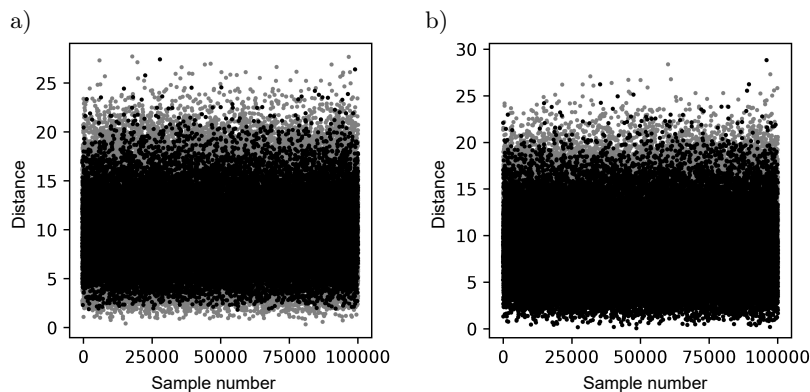
Fig. 18. Distance between the randomized energy matrices and the original energy matrix.
Result for the line weld and high damping at 160 Hz: a) with bias; b) with bias removed.
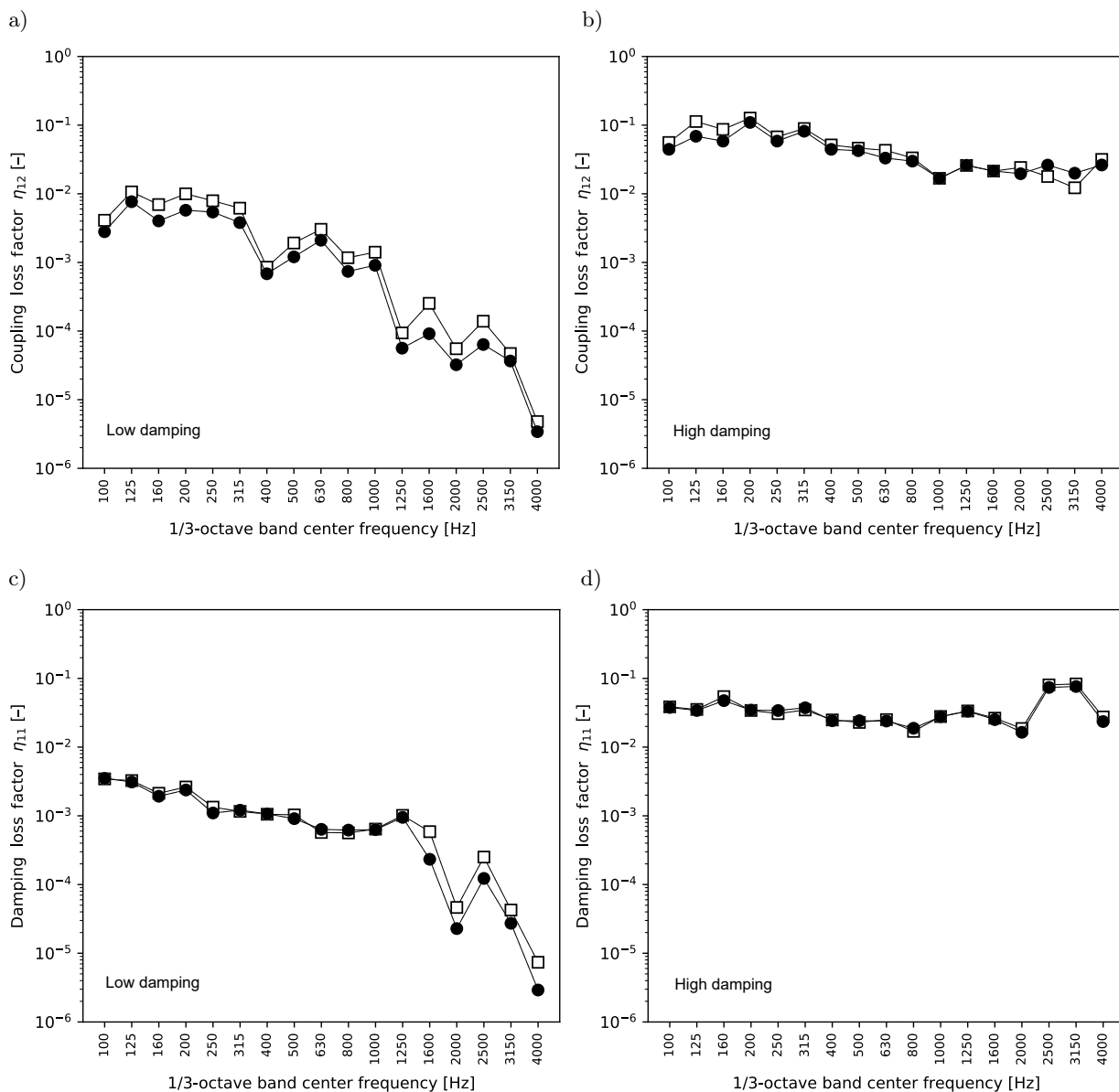

Fig. 19. Effect if removing the bias on the LF values. Results for the line weld: a) CLF at low damping;
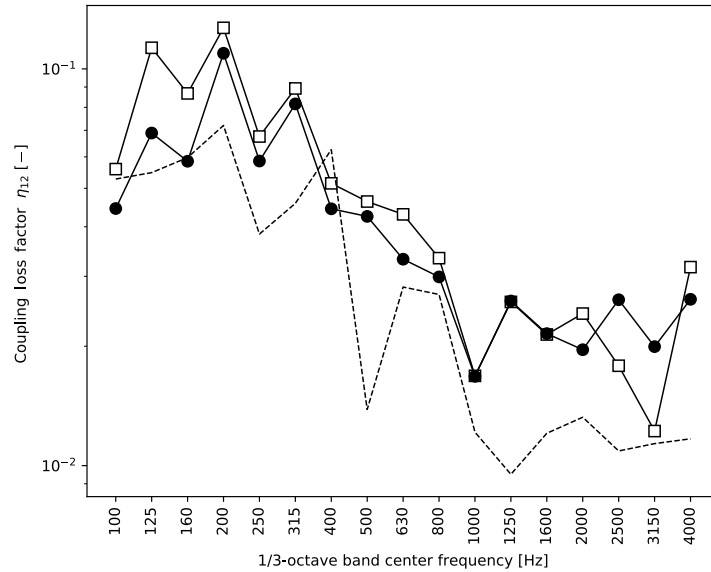b) CLF at high damping; c) DLF at low damping; d) DLF at high damping.

Fig. 20. Results in Fig. 19b compared with the FEM simulation. The experimental result with bias (□),
experimental result without bias (•), FEM simulation (- - -).

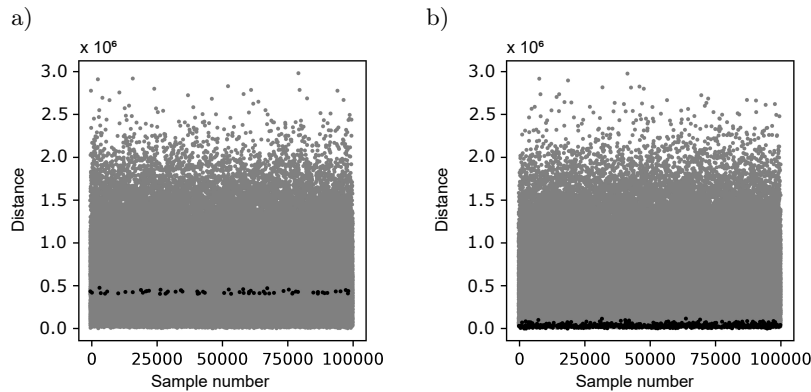a)   b)

Fig. 21. Distance between the randomized energy matrices and the original energy matrix.
Result for the line weld and low damping at 2500 Hz: a) with bias; b) with bias removed.

met and not met. After performing MCF, all negative values were successfully corrected. It seems that MCF can correct negative LFs, irrespective of whether SEA conditions are met or not.

It was observed that the LFs calculated from the bias-free MCF simulation show better agreement with the FEM simulation for frequency bands where the initial bias was significant. For frequency bands where the initial bias was slight, the removal of bias did not significantly alter the LFs. Based on this, it seems reasonable to remove bias each time the MCF procedure is performed.

Acknowledgments

References

1. Bhagwan M.M., Popuri B. (2019), Estimation of coupling loss factors for rectangular plates with different materials and junctions, *Noise & Vibration Worldwide*, **50**(9–11): 306–312, doi: 10.1177/0957456519883264.

2. Bies D.A., Hamid S. (1980), In situ determination of loss and coupling loss factors by the power injection method, *Journal of Sound and Vibration*, **70**(2): 187–204, doi: 10.1016/0022-460X(80)90595-7.

3. Borello G. (2018), Prediction of sound transmission in aircraft over the mid and high frequency range, [in:] *Inter-Noise and Noise-Con Congress and Conference Proceedings*, **258**(2): 5115–5124.

4. Bouhaj M., von Estorff O., Peiffer A. (2017), An approach for the assessment of the statistical aspects of the SEA coupling loss factors and the vibrational energy transmission in complex aircraft structures: Experimental investigation and methods benchmark, *Journal of Sound and Vibration*, **403**: 152–172, doi: 10.1016/j.jsv.2017.05.028.

5. Cacciolati C., Guyader J.L. (1994), Measurement of SEA coupling loss factors using point mobilities, *Philosophical Transactions of the Royal Society of London. Series A: Physical and Engineering Sciences*, **346**(1681): 465–475, doi: 10.1098/rsta.1994.0029.

6. Chen X., Wang D., Ma Z. (2012), Simulation on a car interior aerodynamic noise control based on statistical energy analysis, *Chinese Journal of Mechanical Engineering*, **25**(5): 1016–1021.

7. Cimerman B., Bharj T., Borello G. (1997), Overview of the experimental approach to statistical energy analysis, [in:] *SAE Noise and Vibration Conference and Exposition*, doi: 10.4271/971968.

8. Craik R.J.M. (1982), The prediction of sound transmission through buildings using statistical energy analysis, *Journal of Sound and Vibration*, **82**(4): 505–516, doi: 10.1016/0022-460X(82)90404-7.

9. Culla A., Sestieri A. (2006), Is it possible to treat confidentially SEA the wolf in sheep's clothing?, *Mechanical Systems and Signal Processing*, **20**(6): 1372–1399, doi: 10.1016/j.ymssp.2005.02.007.

10. de las Heras M.J.F., Chimeno M., Millán E.R., Hidalgo F.S. (2018), On the influence of the condition number on the resolution of an ESEA model, [in:] *Inter-Noise and Noise-Con Congress and Conference Proceedings*, **257**(1): 153–161.

11. de las Heras M.J.F., Manguán M.C., Millán E.R., de las Heras L.J.F., Hidalgo F.S. (2020), Determination of SEA loss factors by Monte Carlo Filtering, *Journal of Sound and Vibration*, **479:** 115348, doi: 10.1016/j.jsv.2020.115348.

12. Fahy F.J., Ruivo H.M. (1997), Determination of statistical energy analysis loss factors by means of an input power modulation technique, *Journal of Sound and Vibration*, **203**(5): 763–779, doi: 10.1006/jsvi.1996.0892.

13. Finnveden S. (2011), A quantitative criterion validating coupling power proportionality in statistical energy analysis, *Journal of Sound and Vibration*, **330**(1): 87–109, doi: 10.1016/j.jsv.2010.08.003.

14. Gu J., Sheng M. (2015), Improved energy ratio method to estimate coupling loss factors for series coupled structure, *Journal of Mechanical Engineering*, **45**(1): 37–40, doi: 10.3329/jme.v45i1.24382.

15. Hattori K., Nakamachi K., Sanada M. (1985), Prediction of underwater sound radiated from ship's hull by using statistical energy analysis, *Proceedings of Inter-Noise 85*, Vol. II, p. 645.

16. Hodges C.H., Nash P., Woodhouse J. (1987), Measurement of coupling loss factors by matrix fitting: An investigation of numerical procedures, *Applied Acoustics*, **22**(1): 47–69, doi: 10.1016/0003-682X(87)90015-6.

17. Hopkins C. (2002), Statistical energy analysis of coupled plate systems with low modal density and low modal overlap, *Journal of Sound and Vibration*, **251**(2): 193–214, doi: 10.1006/jsvi.2001.4002.

18. Hwang H.J. (2002), Prediction and validation of high frequency vibration responses of NASA Mars Pathfinder spacecraft due to acoustic launch load using statistical energy analysis, *NASA Technical Reports Server*.

19. Ji L., Sheng X., Xiao X., Wen Z., Jin X. (2015), A review of mid-frequency vibro-acoustic modelling for high-speed train extruded aluminium panels as well as the most recent developments in hybrid modelling techniques, *Journal of Modern Transportation*, **23**(3): 159–168, doi: 10.1007/s40534-015-0080-4.

20. Lafont T., Totaro N., Le Bot A. (2014), Review of statistical energy analysis hypotheses in vibroacoustics, *Proceedings of the Royal Society A: Mathematical, Physical and Engineering Sciences*, **470**(2162): 20130515, doi: 10.1098/rspa.2013.0515.

21. Lalor N. (1990), Practical Consideration for the Measurement of Internal and Coupling Loss Factors on Complex Structures, *ISVR Technical Report*.

22. Lalor N. (1996), Experimental statistical energy analysis: A tool for the reduction of machinery noise, *The Journal of the Acoustical Society of America*, **99**(4): 2568–2574, doi: 10.1121/1.415057.

23. Le Bot A. (2015), *Foundation of Statistical Energy Analysis in Vibroacoustics*, Oxford University Press, United Kingdom.

24. Lyon R.H., DeJong R.G., (1995), *Theory and Application of Statistical Energy Analysis*, Elsevier.

25. Mandale M.B., Bangaru Babu P., Sawant S.M. (2016), Statistical energy analysis parameter estimation for different structural junctions of rectangular plates, *Proceedings of the Institution of Mechanical Engineers, Part C: Journal of Mechanical Engineering Science*, **230**(15): 2603–2610, doi: 10.1177/0954406215615628.

26. Ming R. (1998), The measurement of coupling loss factors using the structural intensity technique, *The Journal of the Acoustical Society of America*, **103**(1): 401–407, doi: 10.1121/1.421096.

27. Nieradka P., Dobrucki A. (2018), Insertion loss of enclosures with lined slits, [in:] *Euronoise 2018-Conference Proceedings*.

28. Pankaj A.C. (2019), *Numerical and Experimental Investigations on Damage Detection in Joints Based on Statistical Energy Analysis like Approach*, Ph.D. Thesis, Department of Mechanical Engineering, National Institute of Technology Karnataka, Surathkal.

29. Panuszka R., Wiciak J., Iwaniec M. (2005), Experimental assessment of coupling loss factors of thin rectangular plates, *Archives of Acoustics*, **30**(4): 533–551.

30. Price A.J., Crocker M.J. (1970), Sound transmission through double panels using statistical energy analysis, *The Journal of the Acoustical Society of America*, **47**(3A): 683–693, doi: 10.1121/1.1911951.

31. Smith Jr. P.W. (1979), Statistical models of coupled dynamical systems and the transition from weak to

strong coupling, *The Journal of the Acoustical Society of America*, **65**(3): 695–698, doi: 10.1121/1.382481.

32. Yap F.F., Woodhouse J. (1996), Investigation of damping effects on statistical energy analysis of coupled structures, *Journal of Sound and Vibration*, **197**(3): 351–371, doi: 10.1006/jsvi.1996.0536.

33. Yoganandh M., Nagaraja J., Venkatesham B. (2019), Prediction of insertion loss of lagging in rectangular duct using statistical energy analysis, *Noise Control Engineering Journal*, **67**(6): 438–446, doi: 10.3397/1/376740.

34. Zarate R., Matus E., Lopez M., Ballesteros L. (2017), Design of quieter kitchen appliances: Sound pressure level modeling and validation of a household refrigerator using statistical energy analysis, [in:] *Proceedings of Meetings on Acoustics*, **30**(1): 030009, doi: 10.1121/2.0000632.